Solid Freeform Fabrication 2024: Proceedings of the 35th Annual International Solid Freeform Fabrication Symposium – An Additive Manufacturing Conference Reviewed Paper

Hybrid Directed Energy Deposition of Geometrically-Complex Pressure Vessels for Advanced HIP Canning and Digitally-Driven Powder Metallurgy

Mario Rodriguez[a], Miguel Hoffmann[b], Jesus R. Cruz[a], Alexander Gomez[a,1], Lauren Heinrich[b], Kenton B. Fillingim[b], Stephen Depietro[c], John Philbrick[c], Anton Du Plessis[d,1], Chad Beamer[f], Brian Post[b], Ryan Dehoff[b], Eric MacDonald[a,1], Thomas Feldhausen[b,*]

[a] *The University of Texas at El Paso, TX 79968, USA*
[b] *Manufacturing Science Division, Oak Ridge National Laboratory, TN 37932, USA*
[c] *Exothermics, Inc, NH 03031, USA*
[d] *Stellenbosch University, Matieland 7602, South Africa*
[e] *Object Research Systems Inc, Quebec H3B 1A7, Canada*
[f] *Quintus Technologies LLC, OH 43035, USA*

Abstract

Directed Energy Deposition (DED) is one of the highest production rate additive manufacturing processes, yet it often faces challenges with dimensional accuracy and surface finish compared to powder bed fusion. Fabricating structures with internal cavities using DED is typically constrained unless a five axis motion system is employed, allowing for the maintenance of a normal to gravity orientation during deposition, which is essential for creating overhanging features and completing enclosed cavities. This capability is particularly valuable for applications sich as pressure vessels and geometrically complex hot isostatic pressing (HIP) containers. The present work explores the tool path strategy required to construct a toroidal cylinder with an internal cavity. Leak testing and cross-sectional analysis such as optical microscopy and the Archimedes density test, confirm that the structure is sufficiently pressure'tight and exhibits minimal porosity, making it suitable for use as complex HIP can, thus paving the way for the next generation of multi-material, digitally-driven powder metallurgy.

Keywords: Hybrid Manufacturing, Directed Energy Deposition (DED), HIP Canning, Powder Metallurgy, Additive Manufacturing,

*Corresponding author email: feldhausenta@ornl.gov

1. Introduction

Manufacturing is evolving to leverage simultaneously the benefits of additive manu-facturing (AM) - such as geometric freedom, part customization, and low waste —with the dimensional accuracy and surface finish of machining [1–4]. In hybrid manufacturing, additive and subtractive processes are integrated within a single build chamber, allowing for the creation of features that would be difficult or impossible to achieve with either method alone [5–7]. Examples include internal cavities with machined surfaces [8] and internally embedded components [9, 10].

Directed Energy Deposition (DED), the AM process employed in this study, has been extensively explored since the mid-1990s [11–15] for building metal, ceramic, and polymer structures [6, 16–23]. DED uses powder or wire feedstock melted by a laser, electric arc, or electron beam [24]. In powder-based systems, powder is delivered to the deposition point via a focused inert gas flow, coinciding with a laser source that melts the powder onto the structure [18]. The result is a strong metallurgical bond between layers or to the substrate, offering full spatial control for on-demand alloying, surface coatings, and component repair [21, 25–28].

Hot Isostatic Pressing (HIP) is a commonly used post-processing technique, especially in the qualification of aerospace structures made via AM. HIP enhances the quality of printed structures, particularly those with complex geometries formed by electron beam [29–37] or laser [38–46] Powder Bed Fusion (PBF), as well as DED [47–51] and Material Extrusion [52]. By applying high temperature and pressure simultaneously, HIP densifies structures and homogenizes their microstructure [53]. HIP is effective in closing large pores (up to 3 mm in diameter) in Ti6Al4V and steel structures made by both traditional and additive methods [54–59]. The increased density from HIP improves fatigue performance [60], making it a standard final process for additively manufactured aerospace components [29, 61]. The concept of building HIP cans using AM has been investigated, particularly through PBF. In these studies, shell geometries were fabricated with internal cavities containing trapped, unmelted powder [62, 63], and included the evaluation of fatigue properties [64]. However, these works were limited to a single-material powder, matching the shell material. PBF is currently specialized for small to medium-sized components due to production speed constraints, but HIP offers more significant advantages for large components. In this context, hybrid DED excels, as it can produce larger components with material versatility, though it may require additional post-processing to achieve the desired surface finish and detail. Finally, as laser PBF is not typically performed in a hard vacuum, gasses were included with the trapped powder, which could lead to thermally induced porosity after subsequent high temperature exposure [65, 66]. Further considerations for AM-enabled HIP canning include the requirement for can ma-terials to have good ductility to distort with the consolidation of internal powder but also be sufficiently strong to maintain the pressure.

The present work investigates the capability of hybrid AM to build a metallic pres-surized vessel to enable applications such as rocket fuel tanks, but more specifically for enhancing powder metallurgy by fabricating geometrically complex HIP containers. The digital-driven paradigm of AM can now enable new geometries from CAD directly for use as HIP cans - not be easily fabricated with traditional approaches. Furthermore, AM HIP cans can include features to facilitate the introduction of powders with pre-attached fill tubes, simulation-driven geometry compensation for HIP deformation, varying thickness walls to optimize the final geometry, and multiple chambers to introduce different metals geometrically. These structures, if capable of holding high pressures without leakage, can be: (a) filled with metal powder; (b) evacuated without disturbing the internal powder to reduce thermally induced porosity, and then finally; (c) welded hermetically closed in preparation of HIP for comprehensive consolidation. Consequently, AM can enable a new generation of powder metallurgy in which HIP canning can provide multi-material unique geometries.

2. Methodology

2.1. Materials

AISI Type 316L Stainless Steel (SS316L) was selected for this work due to its relevance in several industrial applications [67] and well-documented properties in prior AM research [22, 68]. SS316L powder was deposited onto a cylindrical (155 x 50 mm) SS316L substrate. The gas-atomized powder (Oerlikon Metco (US) Inc.) had a particle size distribution with percentiles of $D_{10} = 54.02$ µm, $D_{50} = 73.35$ µm and $D_{90} = 114.50$ µm. Helium was selected as the carrier gas for the powder due to its availability in the machine setup.

2.2. Manufacturing Procedure

The component was manufactured on an Okuma MU8000V-L Laser EX hybrid manufacturing system (Figure 1). The DED fabrication process was carried out using parameters established in previous studies, as detailed in Table 1. The internal cylinder was fabricated using an additive turning toolpath, developed by OPEN MIND Technologies AG as a component of its hyperMILL CAM software. The additive turning toolpath allows axisymmetric components with fluctuating wall thickness to be manufactured by employing a combined raster-spiral method.

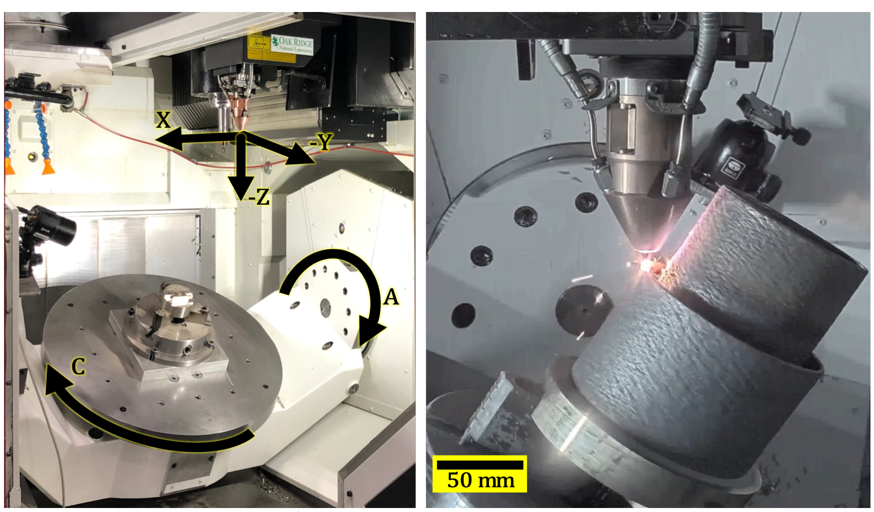

Fig. 1 Okuma MU8000V-L LASER EX five-axis hybrid blown-powder directed energy deposition system (left) and toroidal structure with internal cavity in fabrication (right).

The component was designed to have a height of 165mm, a wall thickness of 4mm, and an inner diameter of 95mm. For the additive turning parameters, the pitch-X and pitch-Z were 2.4mm and 0.66mm [69]. For the outer cylinder, the deposition angle was

Table 1 DED Process Parameters

Parameter	LP-DED
Laser sport diameter (mm)	3.5
Laser power (W)	2,000
Powder feed rate (g/min)	8.6
Traverse feed rate (mm/min)	500*
Layer height (mm)	0.35
Argon shield flow rate (l/min)	10
Helium carrier flow rate (l/min)	5

*Unless noted otherwise

tilted to 30° to avoid obstruction (Figure 2b). Since the outer cylinder was printed at an oblique angle, the traverse speed was adjusted to maintain the proper standoff or distance between the deposition nozzle and deposition surface. An initial traverse feed rate of 900 mm/min was used but was manually adjusted between 500 mm/min and 900mm/min until stabilizing on a final traverse feed rate of 700 mm/min. These adjustments are common in many DED systems and can be detrimental to both geometrical accuracy and metallurgical properties of the final component. However, for HIP cans, the authors expect these changes to be irrelevant if the HIP can hold a vacuum. As the HIP can be removed upon final machining, the minor variance in the processing conditions is expected to be inconsequential.

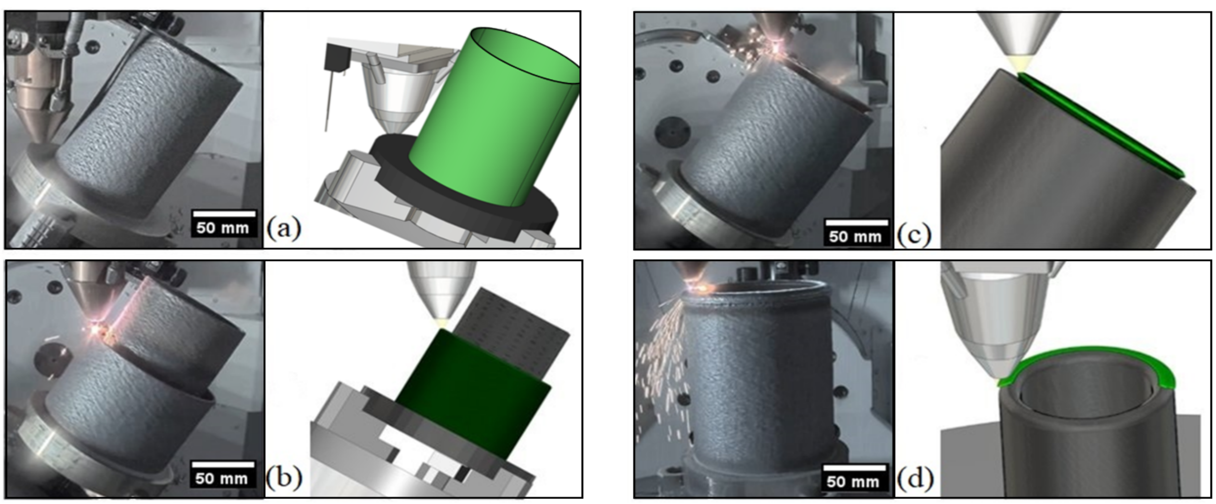

Fig. 2 Steps in the fabrication: a) first interior cylinder; b) second exterior cylinder; c) first of two half arcs; and d) final deposition on the top seam.

The final steps include maintaining a normal with gravity and creating a half arc from the interior cylinder top to span halfway to the exterior cylinder (Figure 2c and Figure 3). A second arc is performed from the external cylinder back to the interior at a rate of 650 mm/min to complete the arch to serve as an unsupported roof of the now cavity. A final additional layer was deposited using a weaving strategy between the two half arcs to close any areas that did not fully fuse and to reinforce the arc structure with a seam at a feed rate of 500 mm/min (Figure 2d). This weave strategy used a pitch of 10 mm and a pitch of 2 mm. The resulting structure, including the build plate, now contains a cylindrical internal chamber which was hypothesized to be capable of handling a vacuum. Additional features such as feed tubes or additional machining could be included for smooth surfaces or prescribed wall thickness as is required. Future work will investigate these and other advantages for HIP for advanced geometrically complex powder metallurgy.

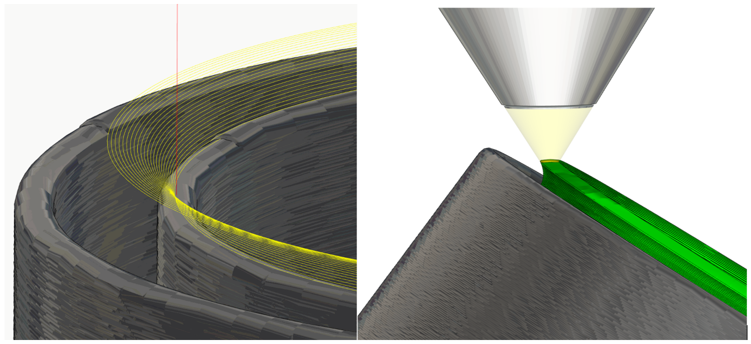

Fig. 3 Tool path for the first arc of the cavity roof printed with constant normal to gravity and schematic of deposition. Path (left) and deposition simulation (right). Yellow lines correspond to G1 (deposition) movement, while the red line corresponds to G0 (reposition) movement.

2.3. Leakage Testing

The vacuum and pressure integrity of the additively manufactured HIP container was verified by methodically spraying helium gas from a nozzle over the container and sealing flange assembly shown in Figure 4 . The sealing flange arrangement was made by tapping a 2mm hole into the build plate and then mounting a face flange and O-ring to make the effect of a vacuum seal. The seal was then mated to a Swagelok tube and bellows connected to a Varian MD30 helium leak detector.

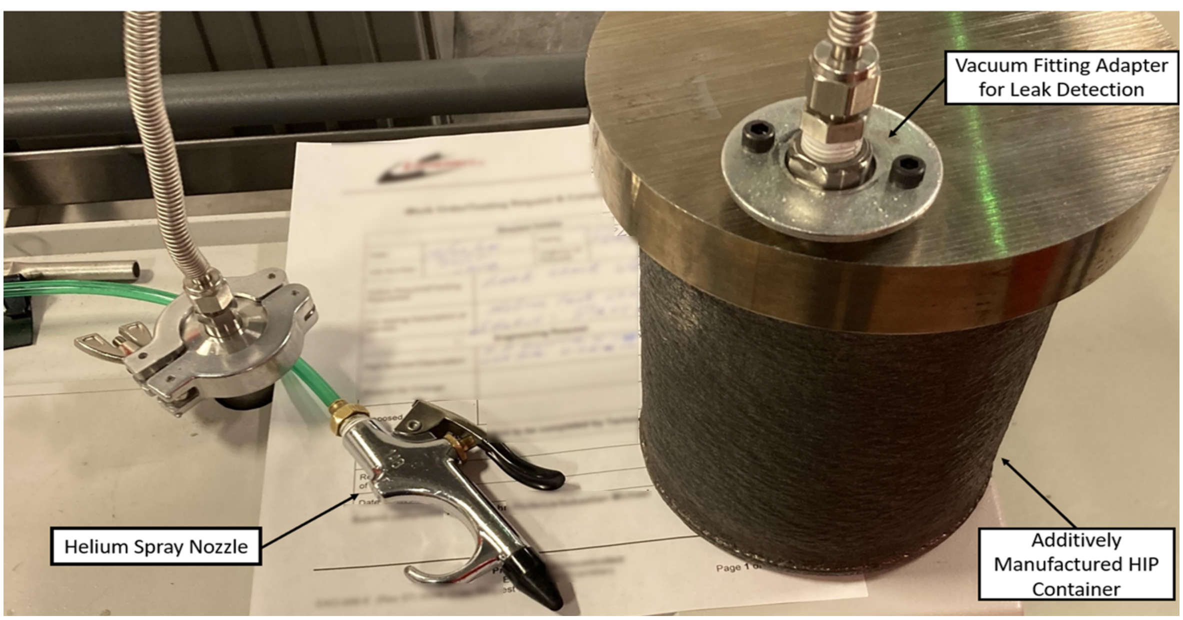

Fig. 4 Vacuum testing setup with DED manufactured cylinder with connected baseplate on top.

2.4. Density and Porosity Characterization

After pressure testing, the container was cross sectioned in half along the XZ plane using a bandsaw. Subsequently, a 30 mm thick slice was removed, and then three samples were obtained by making cuts at 40 mm, 56.5 mm, and 78.5 mm from the slice's top surface, producing a double-walled 40 mm tall arch (sample 1), a 16.5 mm tall external wall (sample 2), and a 22 mm tall external wall (sample 3).

The density and porosity of the samples was evaluated via Archimedes' suspension method [70] and micrographic analysis. Archimedes' method was performed using ethanol at 23 °C with an Ohaus Explorer balance and densities were reported as a percentage of the 8.0 g/cm^3 theoretical density (TD) for SS316L [71, 72]. Samples 1 and 3 were then mounted in epoxy, ground using 500, 800, 1000, and 2000 grit silicon carbide discs in 1 min intervals with water as the lubricant, and then polished using 6, 3, and 1 µm diamond solution with DP-Lubricant Purple in 8 min intervals.

The samples were optically imaged using a Leica DM4000M microscope at a resolution of 1 µm/pixel, employing a brightfield contrasting method with a 5X magnification. The Leica Application Suite X software automatically captured and stitched images of the entire mounted cross-sections into mosaics, enabling the analysis of statistically significant sample sizes. These images were then processed and analyzed using ImageJ®[73]. For porosity characterization, the images were binarized by thresholding to measure pore area, size, and total porosity area fraction (black-to-total pixel ratio). Special focus was placed on the quality of the cavity-roof arch, which was difficult to fabricate due to the oblique deposition angle used to align the DED process with gravity and avoid internal supports.

3. Results and Discussion

The most challenging aspect of this structure was after the completion of the two independent cylinders. Two half arcs were built to span between the cylinders and to provide a sealed cavity. The arcs were created using the tool path shown in Fig. 3, resulting in a non-closed surface remaining after the two operations. A final bead was then deposited to complete the full arch and to provide a sealed and pressure-capable cavity as shown in Fig. 5.

Fig. 5 Fabrication results: (left) after completing inner half arch; (middle) after completing both arches but with gaps remaining; (right) after final bead for complete seal.

3.1. Leakage Testing

Measurements on the sealed additively manufactured container showed a helium leak rate of $\sim 1.0 \times 10^{-9}$ Nml/min or less, indicating sufficient integrity for subsequent HIP trials. By spraying helium around the structure during the cavity vacuum pull, any leaks can be detected, and their locations identified. Future studies will incorporate machining to create precise, thin walls to enhance compliance and ductility for use as a HIP can. In this initial proof-of-concept demonstration, the structure successfully held a vacuum, suggesting that additively manufactured structures have potential for creating geometrically complex HIP cans. During the leak test, we also observed remnant powder from the deposition process inside the enclosed vessel. Despite efforts to remove the excess powder through the vacuum port, complete removal was challenging. This residual powder can damage vacuum test equipment, so future work will focus on developing strategies for powder removal and mitigation.

3.2. Density and Porosity Characterization

After completing the non-destructive leak testing, the part was cross-sectioned to assess the walls and top arch. The cross-section revealed no major defects or issues with the cavity's integrity (Fig. 6). The wall in this example was 3.5 mm thick with rough internal and external surfaces. One advantage of hybrid AM is the ability to machine both internal and external surfaces of cavities, allowing precise control over wall thickness and surface finish for HIP containers. Thinning the walls can enhance the structural ductility needed for effective HIP canning, enabling the container to compress fully and consolidate the internal powder. In contrast, excessively thick and stiff walls could hinder this consolidation during pressing.

AM alone, typically used for near-net shape fabrication, may not achieve the wall thickness precision required for HIP containers. However, by using in situ machining and HIP simulations, wall thickness can be varied to guide solidification shrinkage and ensure the final structure meets the intended geometry. This ability to vary wall thickness, along with creating complex geometric forms, is a key reason for using hybrid AM in the fabrication of HIP containers.

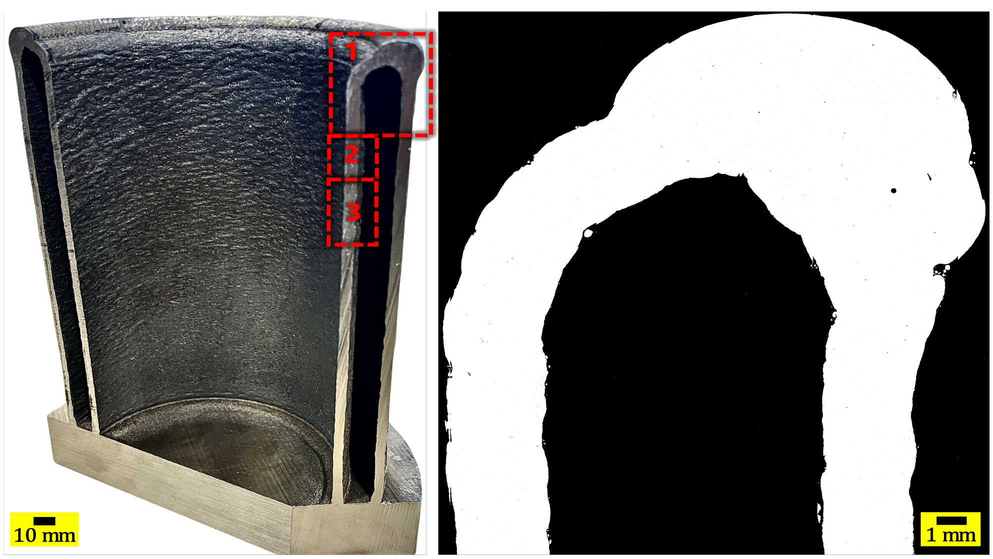

Fig. 6 Manufactured HIP-can : (left) after cross-sectioning, with numbers indicating the samples used for density and porosity characterization; (right) binarized optical micrograph of sample 1.

Based on the quantification of porosity area fraction, samples 1 and 3 were 99.90% and 99.96% dense, respectively. However, the densities derived via Archimedes' method for samples 1-3 were 99.12%, 98.95%, and 99.12%, respectively (Table 2), which are slightly lower than the SS316L densities reported in the DED literature [74–76].

Table 2 Density and Percentage Values by Section

Section	Density (g/cm^3)	%
1	7.92	99.11
2	7.91	98.95
3	7.92	99.118

Sample 1 pores (1,802) measured 6.8 ± 0.8 µm while sample 3's (607) measured 6.4 ± 0.4 µm. Their corresponding pore size distributions (Fig. 7) showed exponential decay with approx. 95% of pores measuring ≤ 30 µm. The remaining 5% of pores, ranging from 30.0-195.2 µm and 30.0-137.9 µm for samples 1 and 3, respectively, let to the lower than expected part density. Compared to sample 3, the higher frequency of pores ≤ 4 µm in sample 1 is attributed to its larger volume.

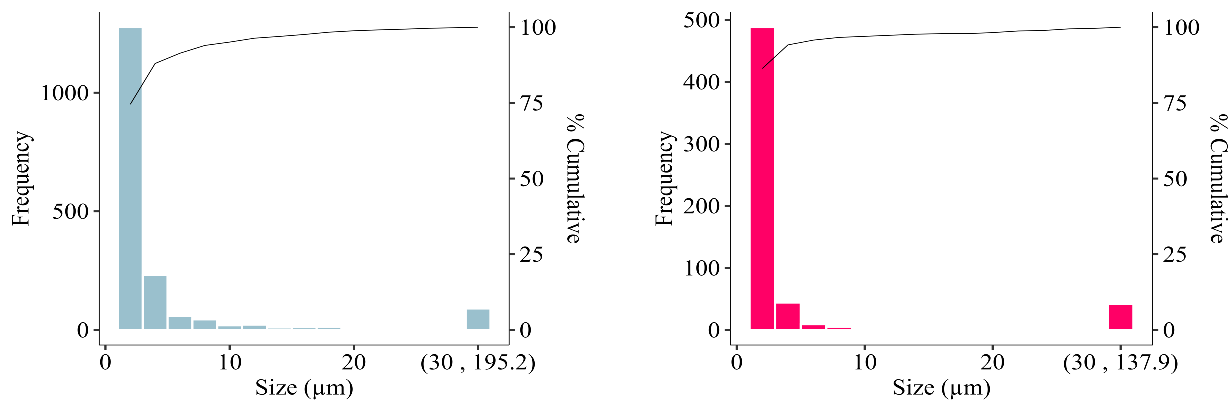

Fig. 7 Pore size distribution for sample 1 (left) and sample 3 (right). Sample numbers correspond to those shown in Fig. 6.

4. Conclusions

The present preliminary investigation demonstrates the potential of a hybrid additive manufacturing system in fabricating complex geometries with vacuum-capable internal cavities, specifically for HIP canning applications. The system's five-axis capabilities successfully produced a structure with complex overhanging features, avoiding the need for support material and showcasing the feasibility of building sophisticated designs. Importantly, the HIP can was effectively designed using an additive turning toolpath, which facilitates the production of axisymmetric components with varying wall thicknesses through a combined raster-spiral technique. Although machining was not required in this proof of concept, the hybrid approach ensures that wall thickness can be meticulously controlled, with internal cavity surfaces accessible for machining during fabrication.

The fabrication process included challenges, particularly in sealing the internal cavity after building two independent cylinders. The application of a final bead after the construction of the half arcs successfully completed the seal, resulting in a pressure-capable cavity. Leak testing confirmed the integrity of the sealed structure, showing a helium leak rate of $\sim 1.0 \times 10^{-9}$ Nml/min, which is sufficient for subsequent HIP trials. The implications of this work are significant for the future of HIP container manufacturing.

Hybrid fabrication enables:

1. Complex, digitally driven HIP can geometries supported by process simulation
2. Variable thickness walls to control and optimize warpage and shrinkage
3. Multiple chambers for multi-material powder metallurgy
4. Inclusion of HIP-can features such as feed tubes to easily weld and seal ports after introducing and evacuating powders and just prior to HIP densification of the final HIP can structure.

Despite the generally slower production rates of additive manufacturing compared to traditional sheet metal welding, the design freedom and digital precision offered by this approach introduce new possibilities for HIP can geometries that are otherwise unattainable. The hybrid process allows for the near-net shape fabrication of multi-chamber shells, with in situ machining to achieve precise dimensional accuracies. Additionally, HIP simulations can preemptively compensate for deformation and shrinkage, further enhancing the potential for complex, multi-material structures. The digitization of the HIP canning process marks a significant advancement in powder metallurgy, paving the way for the next generation of geometrically complex, high-temperature, multi-material structures. Ultimately, hybrid additive manufacturing not only enhances the precision and flexibility of HIP can fabrication but also optimizes consolidation during pressing through the ability to machine surfaces and control wall thickness. These advancements promise to improve yield, quality, and production rates for AM-enabled HIP canning, advancing the field of multi-material, digitally-driven powder metallurgy beyond current capabilities and potentially redefining economic benchmarks in industry.

Acknowledgements

This work was supported by the US Department of Energy, Office of Energy Efficiency and Renewable Energy, Advanced Manufacturing Office under contract number DE-AC05-00OR22725. We would like to highlight the support from the Murchison Chair at the University of Texas at El Paso. AdP is also thankful for financial support from the South African Collaborative Program in Additive Manufacturing (CPAM). The authors are grateful to Dennis Brown from the Manufacturing Demonstration Facility for assisting with machine operations. Additionally, the authors would like to acknowledge the cooperation and support of Open Mind Technologies USA Inc., Carl Zeiss Industrial Metrology LLC, and the Okuma America Corporation.

References

[1] J. L. Dávila, P. I. Neto, P. Y. Noritomi, R. T. Coelho, J. V. L. da Silva, Hybrid manufacturing: a review of the synergy between directed energy deposition and subtractive processes, The International Journal of Advanced Manufacturing Technology 110 (2020) 3377–3390.

[2] K. A. Lorenz, J. B. Jones, D. I. Wimpenny, M. R. Jackson, A review of hybrid manufacturing, in: Solid freeform fabrication conference proceedings, sffsymposium.engr.utexas.edu, 2015, pp. 96–108.

[3] Z. Zhu, V. G. Dhokia, A. Nassehi, S. T. Newman, A review of hybrid manufacturing processes-state of the art and future perspectives, International Journal of Computer Integrated Manufacturing 26 (7) (2013) 596–615.

[4] M. P. Sealy, G. Madireddy, R. E. Williams, P. Rao, M. Toursangsaraki, Hybrid processes in additive manufacturing, Journal of Manufacturing Science and Engineering 140 (2018). doi:10.1115/1.4038644.

[5] T. Yamazaki, Development of a hybrid multi-tasking machine tool: Integration of additive manufacturing technology with cnc machining, Procedia CIRP 42 (2016) 81–86.

[6] J. M. Flynn, A. Shokrani, S. T. Newman, V. Dhokia, Hybrid additive and subtractive machine tools–research and industrial developments, International Journal of Machine Tools and Manufacture 101 (2016) 79–101.

[7] M. Cortina, J. I. Arrizubieta, J. E. Ruiz, E. Ukar, A. Lamikiz, Latest developments in industrial hybrid machine tools that combine additive and subtractive operations, Materials 11 (2018). doi:10.3390/ma11122583.

[8] T. Feldhausen, L. Heinrich, K. Saleeby, A. Burl, B. Post, E. MacDonald, et al., Review of computer-aided manufacturing (cam) strategies for hybrid directed energy deposition, Additive Manufacturing (2022) 102900.

[9] T. Feldhausen, B. Yelamanchi, A. Gomez, K. Saleeby, K. Fillingim, B. Post, et al., Embedding ceramic components in metal structures with hybrid directed energy deposition (2022).

[10] M. Juhasz, R. Tiedemann, G. Dumstorff, J. Walker, A. Du Plessis, B. Conner, W. Lang, E. MacDonald, Hybrid directed energy deposition for fabricating metal structures with embedded sensors, Additive Manufacturing 35 (2020) 101397.

[11] C. Atwood, M. Griffith, L. Harwell, E. Schlienger, M. Ensz, J. Smugeresky, T. Romero, D. Greene, D. Reckaway, Laser engineered net shaping (lens™): A tool for direct fabrication of metal parts, in: International congress on applications of lasers & electro-optics, AIP Publishing, 1998, pp. E1–E7.

[12] G. K. Lewis, E. Schlienger, Practical considerations and capabilities for laser assisted direct metal deposition, Materials and Design 21 (2000) 417–423.

[13] M. L. Griffith, L. D. Harwell, J. T. Romero, Multi-material processing by lens, in: 1997 International, 1997.

[14] N. Shamsaei, A. Yadollahi, L. Bian, S. M. Thompson, An overview of direct laser deposition for additive manufacturing; part ii: Mechanical behavior, process parameter optimization and control, Additive Manufacturing 8 (2015) 12–35.

[15] S. M. Thompson, L. Bian, N. Shamsaei, A. Yadollahi, An overview of direct laser deposition for additive manufacturing; part i: Transport phenomena, modeling and diagnostics, Additive Manufacturing 8 (2015) 36–62.

[16] A. R. Nassar, T. J. Spurgeon, E. W. Reutzel, Sensing defects during directed-energy additive manufacturing of metal parts using optical emissions spectroscopy, in: Solid Freeform Fabrication Symposium Proceedings, University of Texas Austin, TX, 2014.

[17] M. Qian, F. H. Froes, Titanium Powder Metallurgy: Science, Technology and Applications, Elsevier Science, 2015.

[18] K. A. Lorenz, J. B. Jones, D. I. Wimpenny, M. R. Jackson, A review of hybrid manufacturing, in: Solid Freeform Fabrication Conference Proceedings, sffsymposium.engr.utexas.edu, 2015.

[19] J. Keist, K. Taminger, T. A. Palmer, Structure-property correlations for additively manufactured ti-6al-4v components produced using directed energy deposition processes, in: V. Venkatesh, A. Pilchak, J. Allison, S. Ankem, R. Boyer, J. Christodoulou, et al. (Eds.), Proceedings of the 13th World Conference on Titanium, John Wiley & Sons, Inc., 2016, pp. 1395–1400.

[20] V. K. Balla, S. Bose, A. Bandyopadhyay, Processing of bulk alumina ceramics using laser engineered net shaping, International Journal of Applied Ceramic Technology 5 (2008) 234–242.

[21] V. K. Balla, P. D. DeVasConCellos, W. Xue, S. Bose, A. Bandyopadhyay, Fabrication of compositionally and structurally graded ti–tio2 structures using laser engineered net shaping (lens), Acta Biomaterialia 5 (2009) 1831–1837.

[22] T. DebRoy, H. L. Wei, J. S. Zuback, T. Mukherjee, J. W. Elmer, J. O. Milewski, A. M. Beese, A. d. Wilson-Heid, A. De, W. Zhang, Additive manufacturing of metallic components–process, structure and properties, Progress in materials science 92 (2018) 112–224.

[23] L. Nickels, Carbon fiber 3d printing propels bike development, Reinforced Plastics 63 (2019) 93–96.

[24] J. J. Lewandowski, M. Seifi, Metal additive manufacturing: A review of mechanical properties, Annual Review of Materials Research 46 (2016) 151–186.

[25] V. K. Balla, P. P. Bandyopadhyay, S. Bose, A. Bandyopadhyay, Compositionally graded yttria-

stabilized zirconia coating on stainless steel using laser engineered net shaping (lenstm), Scripta Materialia 57 (2007) 861–864.
[26] W. Li, J. Zhang, X. Zhang, F. Liou, Effect of optimizing particle size on directed energy deposition of functionally graded material with blown pre-mixed multi-powder, Manufacturing Letters 13 (2017) 39–43.
[27] M. T. Ensz, M. L. Griffith, D. E. Reckaway, Critical issues for functionally graded material deposition by laser engineered net shaping (lens), in: Proceedings of the 2002 MPIF Laser Metal Deposition Conference, San Antonio, TX, 2002, pp. 8–10.
[28] B. E. Carroll, R. A. Otis, J. P. Borgonia, J.-o. Suh, R. P. Dillon, A. A. Shapiro, D. C. Hofmann, Z.-K. Liu, A. M. Beese, Functionally graded material of 304l stainless steel and inconel 625 fabricated by directed energy deposition: Characterization and thermodynamic modeling, Acta Materialia 108 (2016) 46–54.
[29] M. Ahlfors, F. Bahbou, A. Eklund, U. Ackelid, Hip for am-optimized material properties by hip, in: Materials Research Proceedings, mrforum.com, 2019, pp. 1–10.
[30] A. Leicht, M. V. Sundaram, Y. Yao, E. Hryha, L. Nyborg, L.-E. Rännar, et al., As-hip microstructure of ebm fabricated shell components, in: European Congress and Exhibition on Powder Metallurgy European PM Conference Proceedings, The European Powder Metallurgy Association, 2016.
[31] S. Goel, M. Ahlfors, F. Bahbou, S. Joshi, Effect of different post-treatments on the microstructure of ebm-built alloy 718, Journal of Materials Engineering and Performance 28 (2019) 673–680.
[32] M. Seifi, A. A. Salem, D. P. Satko, U. Ackelid, S. L. Semiatin, J. J. Lewandowski, Effects of hip on microstructural heterogeneity, defect distribution and mechanical properties of additively manufactured ebm ti-48al-2cr-2nb, Journal of Alloys and Compounds 729 (2017) 1118–1135.
[33] T. Persenot, G. Martin, R. Dendievel, J.-Y. Buffiére, E. Maire, Enhancing the tensile properties of ebm as-built thin parts: Effect of hip and chemical etching, Materials Characterization 143 (2018) 82–93.
[34] A. M. Hosseini, S. H. Masood, D. Fraser, M. Jahedi, Mechanical properties investigation of hip and as-built ebm parts, in: Advanced Materials Research, Trans Tech Publications, 2012, pp. 216–219.
[35] A. Eklund, M. Ahlfors, F. Bahbou, J. Wedenstrand, Optimizing hip and printing parameters for ebm ti-6al-4v, in: Key Engineering Materials, Trans Tech Publications, 2018, pp. 174–178.
[36] J. Mireles, S. Ridwan, P. A. Morton, J. Hinojos, R. B. Wicker, Analysis and correction of defects within parts fabricated using powder bed fusion technology, Surface Topography: Metrology and Properties 3 (2015) 034002.
[37] F. Medina, Reducing metal alloy powder costs for use in powder bed fusion additive manufacturing: Improving the economics for production, The University of Texas at El Paso, 2013.
[38] Y. Y. Kaplanskii, A. A. Zaitsev, E. A. Levashov, P. A. Loginov, Z. A. Sentyurina, Nial based alloy produced by hip and slm of pre-alloyed spherical powders. evolution of the structure and mechanical behavior at high temperatures, Materials Science and Engineering: A 717 (2018) 48–59.
[39] J. Kunz, A. Kaletsch, C. Broeckmann, Influence of hip post-treatment on the fatigue strength of 316l-steel produced by selective laser melting (slm), in: European Congress and Exhibition on Powder Metallurgy European PM Conference Proceedings, The European Powder Metallurgy Association, 2016.
[40] B. Zhou, J. Zhou, H. Li, F. Lin, A study of the microstructures and mechanical properties of ti6al4v fabricated by slm under vacuum, Materials Science and Engineering: A 724 (2018) 1–10.
[41] X. Yan, R. Lupoi, H. Wu, W. Ma, M. Liu, G. O'Donnell, et al., Effect of hot isostatic pressing (hip) treatment on the compressive properties of ti6al4v lattice structure fabricated by selective laser melting, Materials Letters 255 (2019) 126537.
[42] N. E. Uzan, S. Ramati, R. Shneck, N. Frage, O. Yeheskel, On the effect of shot-peening on fatigue resistance of alsi10mg specimens fabricated by additive manufacturing using selective laser melting (am-slm), Additive Manufacturing 21 (2018) 458–464.
[43] V. Chastand, P. Quaegebeur, W. Maia, E. Charkaluk, Comparative study of fatigue properties of ti-6al-4v specimens built by electron beam melting (ebm) and selective laser melting (slm), Materials Characterization 143 (2018) 76–81.
[44] M. L. Montero-Sistiaga, S. Pourbabak, J. Van Humbeeck, D. Schryvers, K. Vanmeensel, Microstructure and mechanical properties of hastelloy x produced by hp-slm (high power selective laser melting), Materials & Design 165 (2019) 107598.
[45] A. Mostafa, I. Picazo Rubio, V. Brailovski, M. Jahazi, M. Medraj, Structure, texture and phases in 3d printed in718 alloy subjected to homogenization and hip treatments, Metals 7 (2017) 196.
[46] W. Schneller, M. Leitner, S. Springer, F. Grün, M. Taschauer, Effect of hip treatment on microstruc-

ture and fatigue strength of selectively laser melted alsi10mg, Journal of Materials Processing and Manufacturing Science 3 (2019) 16.
[47] J. S. Keist, S. Nayir, T. A. Palmer, Impact of hot isostatic pressing on the mechanical and microstructural properties of additively manufactured ti–6al–4v fabricated using directed energy deposition, Materials Science and Engineering: A 787 (2020) 139454.
[48] D. R. Waryoba, J. S. Keist, C. Ranger, T. A. Palmer, Microtexture in additively manufactured ti-6al-4v fabricated using directed energy deposition, Materials Science and Engineering: A 734 (2018) 149–163.
[49] Y. Li, X. Lin, Y. Hu, X. Gao, J. Yu, M. Qian, et al., Microstructure and isothermal oxidation behavior of nb-ti-si-based alloy additively manufactured by powder-feeding laser directed energy deposition, Corrosion Science 173 (2020) 108757.
[50] B. J. Hayes, B. W. Martin, B. Welk, S. J. Kuhr, T. K. Ales, D. A. Brice, et al., Predicting tensile properties of ti-6al-4v produced via directed energy deposition, Acta Materialia 133 (2017) 120–133.
[51] Y. Zhou, Z. Wang, X. Lin, Z. Jian, Y. Liu, Y. Ren, et al., Impact toughness and fractography of diverse microstructure in al-cu alloy fabricated by arc-directed energy deposition, Additive Manufacturing 63 (2023) 103414.
[52] Y. Wang, L. Zhang, X. Li, Z. Yan, On hot isostatic pressing sintering of fused filament fabricated 316l stainless steel – evaluation of microstructure, porosity, and tensile properties, Materials Letters 296 (2021) 129854.
[53] H. V. Atkinson, S. Davies, Fundamental aspects of hot isostatic pressing: An overview, Metallurgical and Materials Transactions A 31 (2000) 2981–3000.
[54] A. du Plessis, P. Rossouw, Investigation of porosity changes in cast ti6al4v rods after pressing, Journal of Materials Engineering and Performance 24 (2015) 3137–3141.
[55] C. Cai, B. Song, P. Xue, Q. Wei, C. Yan, Y. Shi, A novel near α-ti alloy prepared by hot isostatic pressing: Microstructure evolution mechanism and high temperature tensile properties, Materials & Design 106 (2016) 371–379.
[56] C. Cai, B. Song, P. Xue, Q. Wei, J.-M. Wu, W. Li, et al., Effect of hot isostatic pressing procedure on performance of ti6al4v: Surface qualities, microstructure and mechanical properties, Journal of Alloys and Compounds 686 (2016) 55–63.
[57] C. Cai, X. Gao, Q. Teng, M. Li, K. Pan, B. Song, et al., A novel hybrid selective laser melting/hot isostatic pressing of near-net shaped ti-6al-4v alloy using an in-situ tooling: Interfacial microstructure evolution and enhanced mechanical properties, Materials Science and Engineering: A 717 (2018) 95–104.
[58] K. Chadha, Y. Tian, J. Spray, C. Aranas, Microtextural characterization of additively manufactured ss316l after hot isostatic pressing heat treatment, Metals and Materials International 28 (2022) 237–249.
[59] E. K. Li, P. D. Funkenbusch, Hot isostatic pressing (hip) of powder mixtures and composites: Packing, densification, and microstructural effects, Metallurgical and Materials Transactions A 24 (1993) 1345–1354.
[60] H. Masuo, Y. Tanaka, S. Morokoshi, H. Yagura, T. Uchida, Y. Yamamoto, et al., Influence of defects, surface roughness and hip on the fatigue strength of ti-6al-4v manufactured by additive manufacturing, International Journal of Fatigue 117 (2018) 163–179.
[61] M. Seifi, M. Gorelik, J. Waller, N. Hrabe, N. Shamsaei, S. Daniewicz, et al., Progress towards metal additive manufacturing standardization to support qualification and certification, JOM 69 (2017) 439–455.
[62] A. du Plessis, B. Yelamanchi, C. Fischer, J. Miller, C. Beamer, K. Rogers, et al., Productivity enhancement of laser powder bed fusion using compensated shelled geometries and hot isostatic pressing, Advances in Industrial and Manufacturing Engineering (2021) 100031.
[63] A. du Plessis, E. Macdonald, Hot isostatic pressing in metal additive manufacturing: X-ray tomography reveals details of pore closure, Additive Manufacturing (2020) 101191.
[64] A. du Plessis, S. Razavi, D. Wan, F. Berto, A. Imdaadulah, C. Beamer, et al., Fatigue performance of shelled additively manufactured parts subjected to hot isostatic pressing, Additive Manufacturing 51 (2022) 102607.
[65] E. Strumza, S. Hayun, S. Barzilai, Y. Finkelstein, R. Ben David, O. Yeheskel, In situ detection of thermally induced porosity in additively manufactured and sintered objects, Journal of Materials Science 54 (2019) 8665–8674.
[66] G. Glatz, L. M. Castanier, A. R. Kovscek, Visualization and quantification of thermally induced porosity alteration of immature source rock using x-ray computed tomography, Energy & Fuels 30

(2016) 8141–8149.

[67] L. Gardner, The use of stainless steel in structures, Progress in Structural Engineering and Materials 7 (2) (2005) 45–55.

[68] A. Saboori, A. Aversa, G. Marchese, S. Biamino, M. Lombardi, P. Fino, Microstructure and mechanical properties of aisi 316l produced by directed energy deposition-based additive manufacturing: A review, Applied sciences 10 (9) (2020) 3310.

[69] T. Feldhausen, R. Kannan, K. Saleeby, J. Haley, T. Kurfess, D. Bourdages, et al., Performance of discontinuity-free components produced by additive turning computer aided manufacturing strategy, Journal of Materials Processing Technology 308 (2022) 117732.

[70] S. W. Hughes, Archimedes revisited: a faster, better, cheaper method of accurately measuring the volume of small objects, Physics education 40 (5) (2005) 468.

[71] M. Yakout, M. Elbestawi, S. C. Veldhuis, Density and mechanical properties in selective laser melting of invar 36 and stainless steel 316l, Journal of Materials Processing Technology 266 (2019) 397–420.

[72] B. Verlee, T. Dormal, J. Lecomte-Beckers, Density and porosity control of sintered 316l stainless steel parts produced by additive manufacturing, Powder Metallurgy 55 (4) (2012) 260–267.

[73] T. Ferreira, W. Rasband, ImageJ user guide, ImageJ/Fiji 1 (2012) 155–161.

[74] M. Hoffmann, L. Heinrich, M. Paramanathan, K. B. Fillingim, A. Elwany, T. Feldhausen, Hybrid additive manufacturing of aisi 316l via asynchronous powder and hot-wire laser directed energy deposition, Journal of Manufacturing Processes 127 (2024) 446–456.

[75] J. Yu, M. Rombouts, G. Maes, Cracking behavior and mechanical properties of austenitic stainless steel parts produced by laser metal deposition, Materials & Design 45 (2013) 228–235.

[76] Z. E. Tan, J. H. L. Pang, J. Kaminski, H. Pepin, et al., Characterisation of porosity, density, and microstructure of directed energy deposited stainless steel aisi 316l, Additive Manufacturing 25 (2019) 286–296. doi:10.1016/j.addma.2018.11.014.